JOURNAL OF APPLIED ELECTROCHEMISTRY 17 (1987) 1267–1280

Mechanism of copper–nickel alloy electrodeposition

E. CHASSAING, K. VU QUANG

Centre d'Etudes de Chimie Métallurgique du CNRS, 15 rue Georges Urbain, 94407 Vitry/Seine, France

R. WIART

Laboratoire propre no 15 du CNRS, 'Physique des Liquides et Electrochimie', associé à l'Université Pierre et Marie Curie, 4 Place Jussieu, 75252 Paris Cedex 05, France

Received 26 February 1987; revised 12 May 1987

The codeposition kinetics of copper and nickel alloys in complexing citrate ammonia electrolytes has been investigated by means of polarization and electrochemical impedance techniques. It is confirmed that the two-step discharge of the complexed cupric species Cu(II)Cit is diffusion-controlled during the alloy deposition, resulting in an increase in the nickel content of the alloy with electrode polarization. Impedance spectra are also consistent with a two-step discharge of Ni(II) cations involving an intermediate adsorbate, $Ni(I)_{ads}$, originating from the reversible first step. A reaction model is developed for the parallel discharge of Cu(II)Cit and Ni(II) in which the reactions for nickel deposition are catalysed by active sites permanently renewed at the surface of the growing alloy. The surface density of these sites, slowly nucleated from $Ni(I)_{ads}$ and included in the deposit, varies with the electrode polarization, thus generating a low-frequency feature specific of Cu–Ni codeposition. This reaction model reproduces to a reasonable extent the potential dependence of the partial current densities for nickel and copper discharge, the current dependence of the alloy nickel content and also most of the experimental relaxation processes observed on impedance spectra.

Nomenclature

b_1, b_2, b_3, b_3', b_4, b_5, b_7	Tafel coefficients (V^{-1})
$\mathscr{C}$	concentration of Cu(II)Cit at distance x ($mol\,cm^{-3}$)
[Cu(II)]	bulk concentration of Cu(II)Cit ($mol\,cm^{-3}$)
$\mathscr{C}_0$	concentration of Cu(II)Cit at $x = 0$ ($mol\,cm^{-3}$)
$\mathscr{C}^*$	concentration of Cu(I)Cit at $x = 0$ ($mol\,cm^{-3}$)
$\Delta\mathscr{C}_0$, $\Delta\mathscr{C}^*$	variations in $\mathscr{C}_0$, $\mathscr{C}^*$ due to ΔE
(Cu), (Ni)	molecular weights (g)
C_{dl}	double layer capacitance ($F\,cm^{-2}$)
D	diffusion coefficient of Cu(II)Cit ($cm^2\,s^{-1}$)
E	electrode potential (V)
f	frequency (s^{-1})
F	Faraday (constant 96 487 A s mol^{-1})
g	interaction factor between adsorbates
i, i_{Cu}, i_{Ni}	current densities ($A\,cm^{-2}$)
$Im(Z)$	imaginary part of Z
j	$(-1)^{1/2}$
k	mass transfer coefficients ($cm\,s^{-1}$)
K_1, K_3	rate constants ($cm\,s^{-1}$)
K_2	rate constant (s^{-1})
K_3', K_4, K_5, K_6, K_7	rate constants ($cm^{-2}\,s^{-1}$)
[Ni(II)]	bulk concentration of $NiSO_4$ ($mol\,cm^{-3}$)
R_t	charge transfer resistance ($\Omega\,cm^2$)
$Re(Z)$	real part of Z
t	time (s)
x	distance from the electrode (cm)
Z_F	faradaic impedance ($\Omega\,cm^2$)
Z	electrode impedance
β	maximal surface concentration of

0021–891X/87 $03.00 + .12

	$Ni(I)_{ads}$ intermediates (mol cm^{-1})	$\Delta\theta_1$, $\Delta\theta_2$	variations in θ_1, θ_2 due to ΔE
γ	nickel content in the deposited alloy (wt %)	τ^*	$= K_2^{-1}$ (s)
		τ_d	diffusion time constant (s)
δ	thickness of Nernst diffusion layer (cm)	τ_1	time constant relative to θ_1 (s)
		τ_2	time constant relative to θ_2 (s)
θ_1	electrode coverage by adsorbed $Ni(I)_{ads}$ intermediate	ω	angular frequency (rad s^{-1})
		Ω	electrode rotation speed (rev min^{-1})
θ_2	electrode coverage by active sites		

1. Introduction

Copper–nickel alloys are known to be highly corrosion resistant, especially the commercial Monel alloys that contain about 70% nickel. The plating of Cu–Ni alloys has long raised interest because of its potential in corrosion protection as well as for decorative purpose. Electrolysis using direct or pulse current has been developed on a laboratory scale which enables plating of thick, crack-free and compact deposits of determined composition [1, 2]. To achieve the codeposition of nickel and copper, the addition of complexing agents is necessary to diminish the gap between the reduction potentials of Ni(II) and Cu(II) species; trisodium citrate and ammonia seem to be among the most efficient compounds [3–5].

So far few investigations have been devoted to the kinetics of alloy electrodeposition. Only polarization techniques have been used for the study of Cu–Ni plating [4, 5]. The role of the hydrodynamic regime was thus emphasized which showed that Cu–Ni alloy formation was achieved under limiting current density for Cu(II) reduction [5]. However, no reaction path has been proposed so far. In previous work concerning the role of citrate and citrate–ammonia complexing agents on copper electrocrystallization, it has been shown that the complexing agents adsorb and inhibit the reduction of cupric complexing species; a reaction path for copper electrocrystallization has been developed [6]. In the present work the codeposition kinetics of copper and nickel alloys has been studied by means of polarization and electrochemical impedance techniques.

2. Experimental procedure

The electrolytes were made up of Analar grade purity chemicals: 0.025–0.1 M $CuSO_4 \cdot 5H_2O$, 0.4–0.6 M $NiSO_4 \cdot 6H_2O$, 0.7 M trisodium citrate (Na_3Cit) and ammonia up to pH 9.2. The solutions were deaerated by bubbling with U-grade nitrogen and kept at 25° C.

The anode was a large nickel sheet of commercial purity (99.9%) which did not dissolve anodically in sulphate electrolytes. Consequently, the anode purity had no influence on the kinetics of alloy deposition which was also unchanged when using a platinum counter electrode. The cathode was a high-purity copper or nickel disc (0.2 cm^2 in area) rotating at up to 2500 rev min^{-1}. To avoid the current density distribution on a disc electrode giving rise to variations in the alloy composition, copper ring cathodes (inner diameter = 4 mm, outer diameter = 6 mm) were also used. The same polarization curves and impedance spectra versus mean current density were recorded for both ring and disc electrodes.

The current efficiencies were calculated from the weight and composition of the deposited alloy. The copper content of alloy deposits was determined by iodometry after dissolution of the layer plated on a platinum disc (2 cm^2 in area) [7]. The nickel content was obtained by difference. EDAX analysis was also carried out.

The steady-state polarization curves were recorded galvanostatically or potentiostatically and corrected for ohmic drop. All potentials were referred to the saturated sulphate electrode (SSE). The partial polarization curves for copper and nickel reduction were calculated from the deposit composition and current efficiencies. In our experiments the partial hydrogen reduction current can

be disregarded since the current efficiency of alloy deposition was always higher than 95%. Electrochemical impedance plots were recorded within the range 60 kHz to 5 mHz using a frequency response analyser (Solartron 1250) controlled by an Apple microcomputer.

3. Results

3.1. *Polarization curves*

As already reported [5], the complexing effect of trisodium citrate and ammonia added to copper sulphate electrolytes shifts the reduction curve of the cupric species markedly towards more negative potentials (Fig. 1, curves 1 and 2). The partial polarization curve for copper discharge (curve 3) during Cu–Ni codeposition is located at slightly more negative potentials and, furthermore, exhibits a limiting current density lower than that relative to pure copper sulphate electrolytes. A comparison of curves 2 and 3 indicates that the copper discharge is inhibited by the presence of $NiSO_4$. On the other hand, at such a concentration of citrate and pH, the reduction of Ni(II) (curve 5) occurs at approximately the same potential as in pure nickel solutions (curve 4). However for the alloy deposition the partial nickel curve exhibits a larger slope, indicating a catalysing effect of the Cu(II) species on the nickel reduction. The slight inhibition observed at low overpotentials is scarcely significant and might result from an imprecise determination of the deposit composition, especially at low nickel content.

For Cu–Ni codeposition the total and partial polarization curves obtained with increasing $CuSO_4$ concentration are shown in Fig. 2. The electrode polarization is seen to decrease when the copper concentration is increased (curves 1 to 3). The partial copper reduction curves exhibit a limiting current density proportional to the electrolyte $CuSO_4$ concentration (Fig. 3A) and to the square root of the electrode rotation speed (Fig. 3B). This indicates a mass transport control of the copper reduction process. As observed in Fig. 1, the partial current density of copper and its limiting value are much lower than for the separate reduction in pure $CuSO_4$/citrate electrolytes. This indicates a decreased activity and a probably lower diffusion coefficient of the cupric species as a result of the presence of nickel species in the electrolyte.

The partial nickel reduction curve (Fig. 2, curve b) does not depend on the electrode rotation speed nor on the copper sulphate concentration in the ranges investigated. For 0.4 M $NiSO_4$ concentration, nickel codeposition is achieved only for potentials more negative than -1.55 V; the

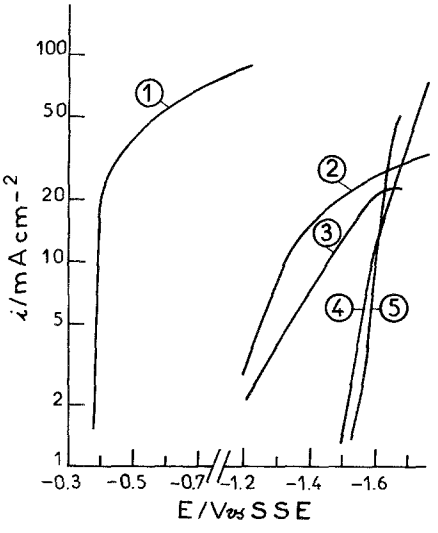

Fig. 1. Steady-state polarization curves. Electrode rotation speed, 500 rev min^{-1}. (1) 0.1 M $CuSO_4$, 0.1 M K_2SO_4; (2) 0.1 M $CuSO_4$, 0.7 M Na_3Cit, pH = 9.6; (3) 0.1 M $CuSO_4$, 0.4 M $NiSO_4$, 0.7 M Na_3Cit, pH = 9.2, partial copper polarization curve; (4) 0.4 M $NiSO_4$, 0.7 M Na_3Cit, pH = 9.3; (5) same electrolyte as for curve 3, partial nickel polarization curve.

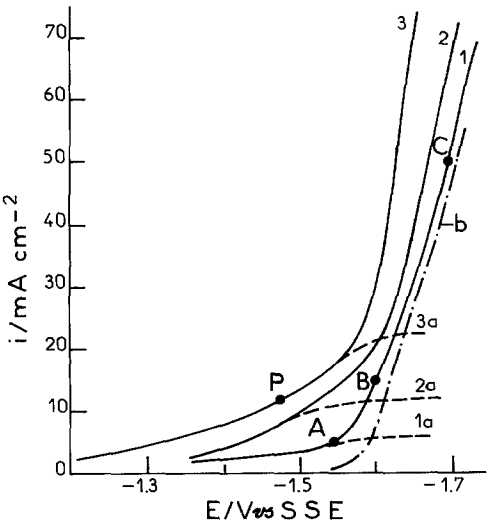

Fig. 2. Steady-state polarization curves in 0.4 M $NiSO_4$, 0.7 M Na_3Cit, pH = 9.2, with increasing $CuSO_4$ concentration: (1) 0.025 M; (2) 0.05 M; (3) 0.1 M. The partial curves are indicated for (a) copper and (b) nickel. Electrode rotation speed, 500 rev min^{-1}.

nickel content in the deposit first increases very steeply with current density up to about 25 mA cm^{-2}, but beyond this value the increase is much less (see Fig. 8).

3.2. *Impedance measurements*

The dependence of the impedance on current density is illustrated in Figs 4 and 5 for two different concentrations and an electrode rotation speed of 500 rev min^{-1}. On all spectra the high-frequency loop corresponds to the charge transfer resistance, R_t, and the double layer capacitance whose value (between 50 and 170 μF cm^{-2}) increases with the electrode polarization. For low polarizations where only copper deposition takes place, the impedance plots exhibit the characteristic features of copper reduction in citrate electrolytes [6], as exemplified in Fig. 4. In addition to the high-frequency loop, a medium-frequency capacitive loop appears showing a characteristic frequency depending on the rotation speed. The R_1/R_t ratio (where R_1 denotes the maximum of the real part of the impedance and R_t the transfer resistance) increases with current density.

As soon as nickel codeposition starts ($E < -1.55$ V for the electrolyte used in Fig. 5), a large inductive feature appears (Fig. 5A). Its characteristic frequency (~ 0.1 Hz) does not depend markedly on the electrode rotation speed nor on the copper sulphate concentration. The frequency increases slightly and the size of the loop decreases for increasingly negative potentials. For $E < -1.6$ V a second inductive feature appears at lower frequencies (Fig. 5B).

For potentials between -1.55 and -1.65 V, a capacitive feature is observed at medium frequencies

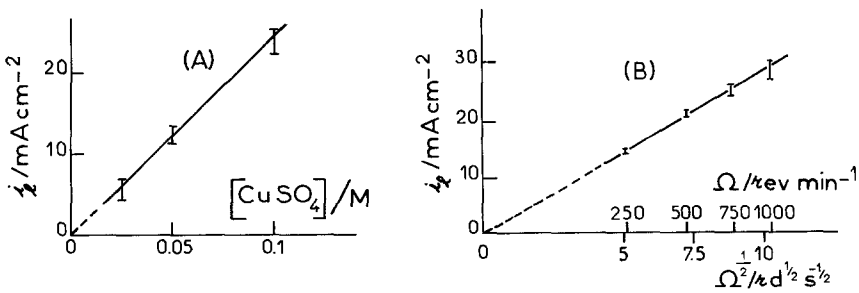

Fig. 3. Limiting current density, i_l, for partial copper reduction versus: (A) $CuSO_4$ bulk concentration (M) at 500 rev min^{-1}; (B) square root of the electrode rotation speed in 0.1 M $CuSO_4$.

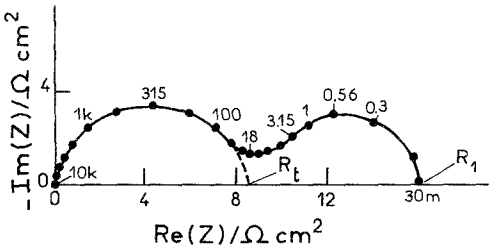

Fig. 4. Complex plane impedance plot recorded in 0.4 M $NiSO_4$, 0.1 M $CuSO_4$, 0.7 M Na_3Cit at pH = 9.2. Electrode rotation speed, 500 rev min^{-1}; electrode polarization $E = -1.47$ V; $i = 12.5$ mA cm^{-2} corresponding to point P in Fig. 2, curve 3.

and separated from the high-frequency loop by a small inductive feature (Fig. 5A, 5B). The characteristic frequency of this small loop is independent of the electrode rotation speed or $CuSO_4$ bulk concentration but increases slightly with overpotential, as already observed for separate nickel deposition in sulphate or chloride electrolytes [8]. The ratio R_l/R_t, strongly dependent on the electrode polarization, increases when the $CuSO_4$ bulk concentration in the bath or the electrode rotation speed is increased (see Fig. 12). The characteristic frequency of this feature increases with copper sulphate concentration and with overpotential but not significantly with the electrode rotation speed (see Fig. 13).

For larger overpotentials ($E < -1.65$ V), the medium-frequency capacitive feature splits and an additional loop appears (Fig. 5C). In this region of potentials, the R_l/R_t ratio increases again with increasing overvoltage (see Fig. 12). This additional capacitive loop is probably associated with the nickel reduction process which is predominant, and its proper frequency is about the same as that of one of the inductive features observed at lower overpotentials.

The current density dependence of the $R_t i$ product exhibits a well-pronounced minimum at a low $CuSO_4$ concentration (Fig. 6, curve 2). It decreases from 90 mV, a value close to that observed for copper discharge in citrate electrolytes [6]. For higher current densities it varies similarly to the $R_t i$ product obtained for pure nickel deposition in citrate–ammonia electrolytes (Fig. 6, curve 1). Experimental data also indicate that the $R_t i$ product increases with the electrode rotation speed and with the copper sulphate concentration in the electrolyte.

4. Discussion

For copper reduction in citrate–ammonia electrolytes [6] the two-step discharge of the complexed cupric species Cu(II)Cit, transported by diffusion to the interface, has to be considered via a soluble

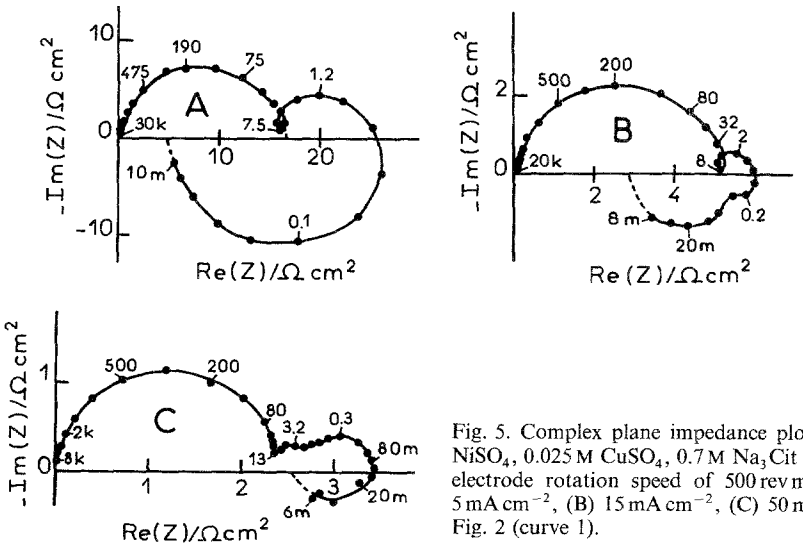

Fig. 5. Complex plane impedance plots recorded in 0.4 M $NiSO_4$, 0.025 M $CuSO_4$, 0.7 M Na_3Cit at pH = 9.2. and an electrode rotation speed of 500 rev min^{-1}, at points (A) 5 mA cm^{-2}, (B) 15 mA cm^{-2}, (C) 50 mA cm^{-2} indicated in Fig. 2 (curve 1).

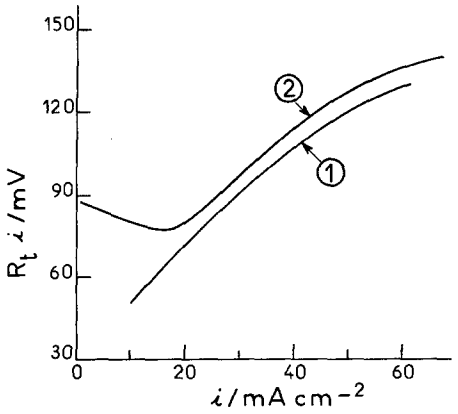

Fig. 6. Current density dependence of the $R_t i$ product. (1) 0.4 M $NiSO_4$, 0.7 M Na_3Cit, pH = 9.2; (2) same electrolyte with addition of 0.025 M $CuSO_4$.

intermediate Cu(I)Cit (reactions 1 and 2, Table 1). The decomplexation yields a surface excess of 'free' complexing agent, denoted Cit, which can either diffuse away or adsorb (reactions K and K') on the electrode surface. This adsorbed complexing agent may inhibit copper deposition on a fraction, θ, of the electrode area, but in the case of Cu–Ni alloy codeposition, with relatively low $CuSO_4$ concentration in the electrolyte, the low-frequency capacitive feature essentially results from the diffusion-controlled discharge of Cu(II)Cit. Therefore, the inhibiting influence of the adsorbed complexing agent Cit can be disregarded and, in the reaction mechanism for the copper discharge, reactions K and K' will be neglected.

$$\begin{array}{ccccc} [\mathrm{Cu(II)Cit}]_b & & & & (\mathrm{Cit})_b \\ \uparrow \mathrm{D} & & & & \mathrm{D} \uparrow \\ [\mathrm{Cu(II)Cit}]_0 + e & \xrightarrow{K_1} & [\mathrm{Cu(I)Cit}]_0 + e & \xrightarrow{K_2} & \mathrm{Cu} + (\mathrm{Cit})_0 \\ & & & & \mathrm{K} \updownarrow \mathrm{K'} \\ & & & & (\mathrm{Cit})_{ads} \end{array}$$

The subscripts 0 and b correspond respectively to the electrode surface and the electrolyte bulk.

Nickel reduction is not dependent on the adsorption of Cit since no capacitive feature has been observed for pure nickel reduction in 0.7 M citrate electrolytes at the same pH (9.2). For nickel

Table 1. Rate constants and Tafel coefficients of reactions and diffusion used for the simulations in Figs 7 to 10

Reaction i	*Rate constant at* E = −1.4 *V*	*Tafel coefficient* (V^{-1})
1. $[\mathrm{Cu(II)Cit}]_0 + e \longrightarrow [\mathrm{Cu(I)Cit}]_0$	$K_1 = 2 \times 10^{-3}\,\mathrm{cm\,s^{-1}}$	$b_1 = 10$
2. $[\mathrm{Cu(I)Cit}]_0 + e \longrightarrow \mathrm{Cu} + (\mathrm{Cit})_0$	$K_2 = 5\,\mathrm{s^{-1}}$	$b_2 = 11$
3. $\mathrm{Ni(II)} + e \rightleftharpoons \mathrm{Ni(I)_{ads}}$	$K_3[\mathrm{Ni(II)}] = 2 \times 10^{-8}\,\mathrm{cm^{-2}\,s^{-1}}$	$b_3 = 11$
	$K_3' = 7.5 \times 10^{-5}\,\mathrm{cm^{-2}\,s^{-1}}$	$b_3' = -28$
4. $\mathrm{Ni(I)_{ads}} + e \longrightarrow \mathrm{Ni}$	$K_4 = 6.4 \times 10^{-7}\,\mathrm{cm^{-2}\,s^{-1}}$	$b_4 = 5$
5. $\mathrm{Ni(I)_{ads}} + n\mathrm{Cu} + e \longrightarrow \mathrm{s}$	$K_5 = 5 \times 10^{-10}\,\mathrm{cm^{-2}\,s^{-1}}$	$b_5 = 15$
6. $\mathrm{s} + \mathrm{Cu} \longrightarrow \mathrm{Cu/s}$	$K_6 = 7.5 \times 10^{-10}\,\mathrm{cm^{-2}\,s^{-1}}$	
7. $\mathrm{s} + \mathrm{Ni(I)_{ads}} + e \longrightarrow \mathrm{Ni/s}$	$K_7 = 2.5 \times 10^{-10}\,\mathrm{cm^{-2}\,s^{-1}}$	$b_7 = 19$
Diffusion of Cu(II)Cit	$k = 2.3 \times 10^{-3}\,\mathrm{cm\,s^{-1}}$	

deposition in sulphate and chloride electrolytes [8], the two-step reduction of Ni(II) (reactions 3 and 4, Table 1) involves the adsorbed intermediate $Ni(I)_{ads}$:

$$Ni(II) + e \underset{K_3'}{\overset{K_3}{\rightleftharpoons}} Ni(I)_{ads} + e \xrightarrow{K_4} Ni$$

This reaction is considered to occur on catalytic active sites, s, nucleated from the $Ni(I)_{ads}$ on the surface of the alloy deposit:

$$Ni(I)_{ads} + nCu + e \xrightarrow{K_5} s$$

An important effect of alloy deposition is the permanent renewal of the active sites consumed by either reaction 6 or reaction 7 (Table 1):

$$s + Cu \xrightarrow{K_6} Cu/s$$

$$s + Ni(I)^{+}_{ads}\, e \xrightarrow{K_7} Ni/s$$

The active sites probably correspond to some particular bonds and/or arrangements between nickel and copper atoms at the electrode surface which give them a particular reactivity. This may result from the association of one nickel atom with several (n) copper atoms (reaction 5). As a consequence of deposition, these catalytic sites propagate along the surface of the growing alloy. Then, reactions 6 and 7 express a deactivation process of these sites occurring when they meet, respectively, an excess in copper atoms or nickel adions on the deposit surface. It is noticeable that reaction 7 can also be regarded as an inclusion process of active sites into the deposit. As compared with reactions 3 and 4, reactions 5, 6 and 7 correspond to slow processes which ensure the slow renewal of sites during the alloy deposition.

For simplicity the following assumptions were adopted.

(i) The diffusion processes for Cu(II)Cit and Cit are governed by Fick's laws.

(ii) The adsorption processes for Cit_{ads} and $Ni(I)_{ads}$ follow the Langmuir isotherm.

(iii) The rate constants for the electrochemical reactions vary with the electrode potential according to Tafel's law: for each i reaction, $K_i = k_i \exp(b_i E)$.

(iv) The discharges of Cu(II)Cit and Ni(II) are independent. However, changes in ion activities may result from the presence of both Cu(II)Cit and Ni(II) in the electrolyte.

4.1. *Equations for copper reduction*

The electron balance for copper discharge yields the partial current density

$$i_{Cu} = F(K_1 \mathscr{C}_0 + K_2 \mathscr{C}^*) \tag{1}$$

At the distance x from the interface, the value of $\mathscr{C}$ is governed by Fick's second law,

$$\frac{\partial \mathscr{C}}{\partial t} = D\left(\frac{\partial^2 \mathscr{C}}{\partial x^2}\right) \tag{2}$$

The boundary conditions for a Nernst diffusion layer of thickness δ are as follows:

$$\text{At } x = \delta, \quad \mathscr{C} = [\text{Cu(II)}]$$

$$\text{At } x = 0, \quad \mathscr{C} = \mathscr{C}_0 \text{ such as } D\left(\frac{\partial \mathscr{C}}{\partial x}\right)_0 = K_1 \mathscr{C}_0 \tag{3}$$

The material balance for the surface concentration, $\mathscr{C}^*$, of the monovalent intermediate Cu(I)Cit is:

$$\frac{d\mathscr{C}^*}{dt} = K_1 \mathscr{C}_0 - K_2 \mathscr{C}^* \tag{4}$$

The steady-state solutions of Equations 2 and 4 give the steady-state concentrations:

$$\mathscr{C}_0 = \frac{k[\mathrm{Cu(II)}]}{K_1 + k} \tag{5}$$

$$\mathscr{C}^* = K_1\mathscr{C}_0/K_2 \tag{6}$$

where $k = D/\delta$ is the mass transfer coefficient.

Then the steady-state current density for copper deposition is given by

$$i_{\mathrm{Cu}} = \frac{2FK_1k[\mathrm{Cu(II)}]}{K_1 + k} \tag{7}$$

With increasing cathode polarization, i_{Cu} tends to the limiting current density, i_1, i.e.

$$i_1 = 2Fk[\mathrm{Cu(II)}] \tag{8}$$

4.2. *Equations for nickel deposition*

By considering reactions 3 and 4 much faster than reactions 5, 6 and 7, the material balances give the following equations:

$$\beta\left(\frac{\mathrm{d}\theta_1}{\mathrm{d}t}\right) = K_5\theta_2 - K_6\theta_1 - K_7\theta_1\theta_2 \tag{9}$$

$$\beta\left(\frac{\mathrm{d}\theta_2}{\mathrm{d}t}\right) = K_3[\mathrm{Ni(II)}](1 - \theta_2) - (K_3' + K_4)\theta_2 \tag{10}$$

Since copper and nickel crystals have close unit cell parameters (3.615 Å and 3.524 Å respectively) the coefficient β can reasonably be taken to be equal to the value of the superficial density of the atoms in the (1 1 1) plane, which is close to the $3 \times 10^{-9}\,\mathrm{mol\,cm^{-2}}$.

Taking into account the catalytic effect of sites, s, on nickel deposition, the electron balance gives the partial current density, i_{Ni}:

$$i_{\mathrm{Ni}} = F\theta_1[K_3[\mathrm{Ni(II)}](1 - \theta_2) + (K_4 - K_3')\theta_2] \tag{11}$$

The steady-state solutions of Equations 9 and 10 yield the coverages,

$$\theta_1 = \frac{K_5\theta_2}{K_6 + K_7\theta_2} \tag{12}$$

$$\theta_2 = \frac{K_3[\mathrm{Ni(II)}]}{K_3[\mathrm{Ni(II)}] + K_3' + K_4} \tag{13}$$

and the steady state current density, i_{Ni}, is

$$i_{\mathrm{Ni}} = 2FK_4\theta_1\theta_2 \tag{14}$$

The nickel content, γ, (in weight) of the deposited alloy can be deduced from the partial current densities,

$$\gamma = \frac{(\mathrm{Ni})i_{\mathrm{Ni}}}{(\mathrm{Ni})i_{\mathrm{Ni}} + (\mathrm{Cu})i_{\mathrm{Cu}}} \tag{15}$$

where (Cu) and (Ni) are the respective molecular weights.

4.3. *Electrode impedance*

Disregarding the hydrogen evolution, the total current density for alloy deposition is given by

$$i = i_{Cu} + i_{Ni} \tag{16}$$

where i_{Cu} and i_{Ni} are given by Equations 1 and 11, respectively.

The faradaic impedance, Z_f, can be calculated by linearizing Equations 1 and 11,

$$\frac{1}{Z_f} = \left[\frac{\partial i}{\partial E}\right] + \left[\frac{\partial i}{\partial \theta_1}\right]\frac{\Delta\theta_1}{\Delta E} + \left[\frac{\partial i}{\partial \theta_2}\right]\frac{\Delta\theta_2}{\Delta E} + \left[\frac{\partial i}{\partial \mathscr{C}_0}\right]\frac{\Delta\mathscr{C}_0}{\Delta E} + \left[\frac{\partial i}{\partial \mathscr{C}^*}\right]\frac{\Delta\mathscr{C}^*}{\Delta E} \tag{17}$$

where the first term is R_t^{-1} such as

$$R_t i = \frac{2(K_1\mathscr{C}_0 + K_4\theta_1\theta_2)}{K_1\mathscr{C}_0(b_1 + b_2) + \theta_1\theta_2[K_3'(b_3 + b_3') + K_4(b_3 + b_4)]} \tag{18}$$

At sufficiently low electrode polarization, where only copper deposition occurs ($\theta_2 \simeq 0$), the $R_t i$ product takes the constant value given by $2/(b_1 + b_2)$. At sufficiently high polarizations, where nickel deposition predominates and becomes irreversible ($K_3' \ll K_4$), the $R_t i$ product tends to a second constant equal to $2/(b_3 + b_4)$.

The partial derivatives in Equation 17 can be calculated from Equations 1 and 11:

$$\frac{\partial i}{\partial \theta_1} = 2FK_4\theta_2 \tag{19}$$

$$\frac{\partial i}{\partial \theta_2} = F\theta_1(K_4 - K_3[\text{Ni(II)}] - K_3') \tag{20}$$

$$\frac{\partial i}{\partial \mathscr{C}_0} = FK_1 \tag{21}$$

$$\frac{\partial i}{\partial \mathscr{C}^*} = FK_2 \tag{22}$$

The terms $\Delta\theta_1/\Delta E$ and $\Delta\theta_2/\Delta E$ are obtained by differentiating Equations 9 and 10, respectively:

$$\frac{\Delta\theta_1}{\Delta E} = \frac{K_6\theta_1(b_5 + \Delta\theta_2/\theta_2\Delta E) + K_7\theta_1\theta_2(b_5 - b_7)}{(K_6 + K_7\theta_2)(1 + j\omega\tau_1)} \tag{23}$$

where

$$\tau_1 = \frac{\beta}{K_6 + K_7\theta_2} \tag{24}$$

$$\frac{\Delta\theta_2}{\Delta E} = \frac{\theta_2[K_3'(b_3 + b_3') + K_4(b_3 - b_4)]}{(K_3[\text{Ni(II)}] + K_3' + K_4)(1 + j\omega\tau_2)} \tag{25}$$

where

$$\tau_2 = \frac{\beta}{K_3[\text{Ni(II)}] + K_3' + K_4} \tag{26}$$

By integrating Equation 2, it follows for $x = 0$ [9] that

$$\frac{\Delta\mathscr{C}_0}{\Delta(\partial\mathscr{C}/\partial x)_0} = -\frac{\delta \tanh (j\omega\tau_d)^{1/2}}{(j\omega\tau_d)^{1/2}} \tag{27}$$

where $\tau_d = \delta^2/D$ is the diffusion time constant.

The term $\Delta\mathscr{C}/\Delta E$ is then obtained by differentiating Equation 3 and combining with Equation 27:

$$\frac{\Delta\mathscr{C}_0}{\Delta E} = \frac{b_1\mathscr{C}_0}{1 + \dfrac{k(j\omega\tau_d)^{1/2}}{K_1 \tanh (j\omega\tau_d)^{1/2}}} \tag{28}$$

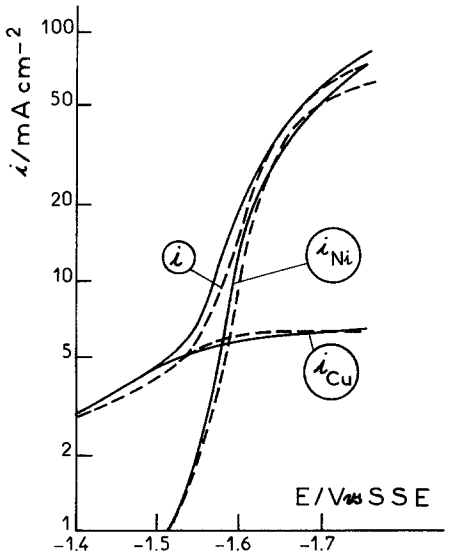

Fig. 7. Partial (i_{Ni} and i_{Cu}) and total (i) polarization curves. Dashed lines: experimental curves for the electrolyte 0.025 M $CuSO_4$, 0.4 M $NiSO_4$, 0.7 M Na_3Cit at pH = 9.2 and an electrode rotation speed of 500 rev min^{-1}. Solid lines: calculated curves for [Cu(II)] = 1.4×10^{-5} mol cm^{-3}, $D = 5 \times 10^{-6}$ cm^2 s^{-1}, $\delta = 22\,\mu$m, and the parameters of reactions given in Table 1.

The term $\Delta\mathscr{C}^*/\Delta E$ is given by differentiating Equation 4:

$$\frac{\Delta\mathscr{C}^*}{\Delta E} = \frac{\mathscr{C}^*(b_1 - b_2 + \Delta\mathscr{C}_0/\mathscr{C}_0\Delta E)}{(1 + j\omega\tau^*)} \tag{29}$$

where

$$\tau^* = \frac{1}{K_2} \tag{30}$$

Finally, Z can be obtained by considering the double layer capacitance, C_{dl}, in parallel with Z_f.

4.4. *Simulations*

From this model, the equations of the polarization curves and impedance plots characteristic of Cu–Ni alloy deposition can be calculated. Fig. 7 gives an example of partial and total polarization curves simulated using the reaction and diffusion parameters given in Table 1. At a rotation speed of 500 rev min^{-1} for the disc electrode, for which $\delta = 22\,\mu$m in water when $D = 5 \times 10^{-6}$ cm^2 s^{-1}, the mass transfer coefficient, k, is 2.3×10^{-3} cm s^{-1}. A bulk concentration [Cu(II)] of Cu(II)Cit species equal to 1.4×10^{-5} mol cm^{-3} has been adopted to fit the limiting current density of partial copper deposition for an electrolyte containing 0.025 M $CuSO_4$ and for $\Omega = 500$ rev min^{-1}. The agreement between experimental data and calculated polarization curves is shown in Fig. 7. The model validity is also evident in Fig. 8 for the variation of the weight of nickel in the deposited alloy as a function of the total current density.

The potential dependences of the coverages θ_1 and θ_2 calculated from Equations 12 and 13, respectively, with the parameters given in Table 1 are shown in Fig. 9. An increase in the coverage θ_2 by $Ni(I)_{ads}$ results from a Tafel coefficient, b_3, of the first charge transfer reaction for nickel deposition which is higher than b_4, for the second charge transfer reaction. The increase in the coverage, θ_1, by sites observed at low electrode polarization is due to the increase in θ_2. A maximum in θ_1 appears near $E = -1.65$ V with a subsequent decrease generated by the situation $b_7 > b_5$.

The polarization dependence of the electrode impedance is illustrated in Fig. 10, where the impedance spectra have been calculated using the same parameters as for Figs 7–9. The high-

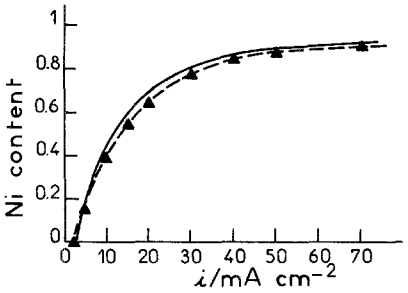

Fig. 8. Current density dependence of the nickel content, y, in the alloy deposit. Dashed line (▲) represents experimental values for the same electrolyte as in Fig. 7. Solid line represents curve with the same parameters as for Fig. 7.

frequency capacitive loop corresponds to R_t in parallel with the double layer capacitance whose value is taken as $100\,\mu F\,cm^{-2}$, corresponding to the mean of experimental data.

The capacitive loop which appears at medium frequencies results from the two-step discharge of Cu(II)Cit species coupled with the diffusion of these species, which is the rate-determining step for copper deposition. Equation 29 indicates that the relaxation process of $\mathscr{C}^*$ exists even when there is no difference between the coefficients b_1 and b_2 because of its coupling with that of $\mathscr{C}_0$. Thus it is normal that the relaxation of $\mathscr{C}^*$ contributes to the capacitive loop on the plots of Fig. 10 which have been simulated with a small difference between b_1 and b_2. It is noteworthy that the adopted values of b_1 and b_2 in the present work are close to those ($11.8\,V^{-1}$) already obtained for pure copper deposition in citrate–ammonia electrolytes [6].

The increasing coverages, θ_1 and θ_2, with electrode polarization in the domain where nickel deposition starts, generate two inductive loops. The first loop, whose proper frequency is ~ 20 Hz and 40 Hz in diagrams B and C of Fig. 10 respectively, is due to the coverage θ_2, and it increases with electrode polarization according to Equation 26. The second loop, which appears near 0.1 Hz on diagram B of Fig. 10, expresses the catalytic effect of sites, s, on the reactions 3 and 4 involved in nickel deposition. Its characteristic frequency also increases slightly with electrode polarization according to Equation 24. For electrode polarizations higher than -1.65 V, the decreasing coverage, θ_1, makes this low-frequency loop become capacitive, as shown in diagram C of Fig. 10.

The calculated variation of the $R_t i$ product with electrode polarization depicted in Fig. 11 (curves 1 and 2) reproduces the minimum value observed when nickel deposition starts reasonably well. The model also agrees with the experimental variations of $R_t i$ with the electrode rotation speed and $CuSO_4$ concentration. On curve 2, calculated by increasing [Cu(II)] and reducing δ, the $R_t i$ minimum is less pronounced, since a larger polarization is necessary to achieve deposits with a high nickel content, thus reducing the reversibility of reaction 3.

The potential dependence of the R_1/R_t ratio which characterizes the size of the medium-frequency capacitive loop is represented in Fig. 12. It first increases due to the increasingly diffusion-controlled kinetics of copper deposition which prevails at low electrode polarizations. The subsequent decrease

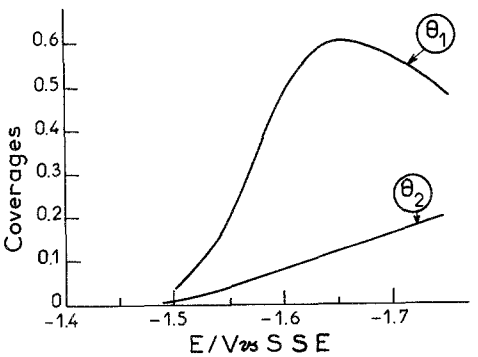

Fig. 9. Potential dependences of the coverages θ_1 and θ_2 calculated with the parameters given in Table 1.

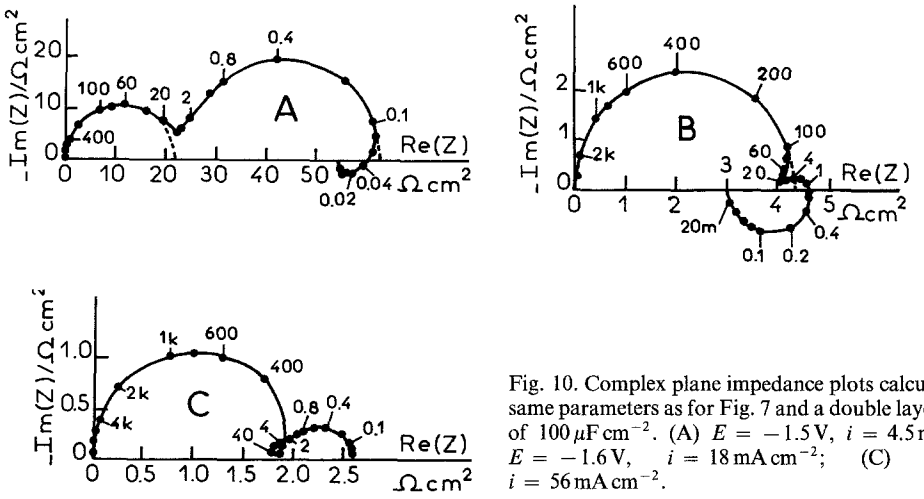

Fig. 10. Complex plane impedance plots calculated with the same parameters as for Fig. 7 and a double layer capacitance of $100\,\mu F\,cm^{-2}$. (A) $E = -1.5\,V$, $i = 4.5\,mA\,cm^{-2}$; (B) $E = -1.6\,V$, $i = 18\,mA\,cm^{-2}$; (C) $E = -1.7\,V$, $i = 56\,mA\,cm^{-2}$.

occurs when nickel codeposition becomes progressively more important. When E reaches $-1.65\,V$, the final increase is connected with the decrease in the coverage, θ_1, by the catalytic sites, s, which generates a capacitive feature. Fig. 12 shows that only a semi-quantitative agreement is achieved between the model and the data obtained under various experimental conditions able to modify the rate of copper deposition.

A semi-quantitative agreement also appears in Fig. 13, which presents the potential dependence of the frequency, f_0, at the apex of this medium-frequency capacitive loop. In spite of a potential-independent value of the diffusion time constant, τ_d, the increase in f_0 originates from both the contribution of the $\mathscr{C}^*$ relaxation, whose proper frequency increases with overpotential according to Equation 30, and the increasing current, i_{Ni}, for nickel deposition added to the current, i_{Cu}, for copper deposition. Such a situation screens the dependence of τ_d upon Ω: the calculated curve is independent of Ω between 500 and $1000\,rev\,min^{-1}$ and it does not account for the increase in f_0 experimentally observed with increasing $CuSO_4$ concentration in the electrolyte.

With the adopted assumptions, the present model still provides an approximate description of the experimental facts. Obviously it does not predict the existence of a second low-frequency inductive loop, as observed in diagrams B and C of Fig. 5. Neither does it yield the splitting of the medium-frequency capacitive feature into the two loops which is observed at high polarizations (see diagram C of Fig. 5). The lack of information about the atomic structure and energetical properties of sites, which might be of several types at the electrode surface, is probably a major reason for the restrictions in the conformity with experimental data. However, this model satisfactorily accounts for a number of experimental results of the relaxation processes observed on impedance diagrams and their potential dependences.

It is noticeable that a clear distinction between the contributions of diffusion and θ_1 decrease to the capacitive loop apparent at high electrode polarizations can be achieved by assuming that the

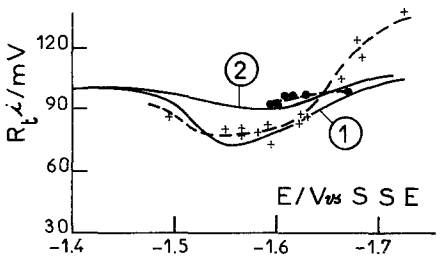

Fig. 11. Potential dependence of the $R_t i$ product. Dashed lines represent experimental curves: (+) electrolyte 1 in Fig. 2, $\Omega = 500\,rev\,min^{-1}$; (●) electrolyte 3 in Fig. 2, $\Omega = 1000\,rev\,min^{-1}$. Solid lines represent calculated curves: (1) with the same parameters as for Fig. 7; (2) by multiplying [Cu(II)] by 4 and dividing δ by $2^{1/2}$.

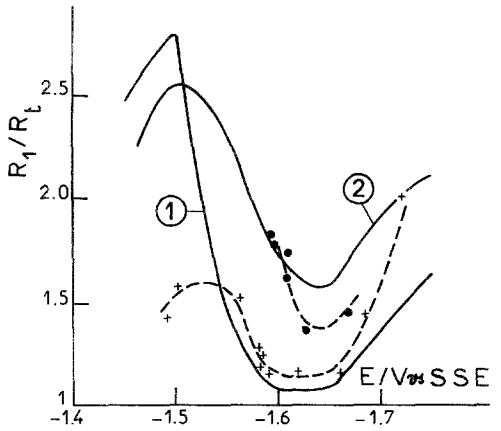

Fig. 12. Potential dependence of the R_1/R_t ratio. Dashed lines represent experimental curves: (+) electrolyte 1 in Fig. 2, $\Omega = 500\,\text{rev min}^{-1}$; (●) electrolyte 3 in Fig. 2, $\Omega = 1000\,\text{rev min}^{-1}$. Solid lines represent calculated curves: (1) with the same parameters as for Fig. 7; (2) by multiplying [Cu(II)] by 4 and dividing δ by $2^{1/2}$.

$Ni(I)_{ads}$ species do not behave independently in the nucleation of sites, and undergo repulsive interactions when their surface coverage, θ_2, exceeds a threshold, θ_0. Therefore, similarly to the formulation previously used for interaction effects [10, 11], the rate, v_5, of reaction 5 is changed from:

$$v_5 = K_5\theta_2 \tag{31}$$

into

$$v_5 = K_5\theta_2 \exp\left[-g(\theta_2 - \theta_0)\right] \tag{32}$$

only for $\theta_2 > \theta_0$. Such a situation is consistent with sites assumed to exist under the form of clusters made of one nickel atom surrounded and bound to several copper atoms. Then the restricted rate, v_5, of formation of sites is sufficient to generate the decrease in θ_1 at high polarizations, and their potential-activated inclusion (reaction 7) can be disregarded. Fig. 14 shows an example of an impedance plot calculated with these assumptions, taking $K_7 = 0$, introducing v_5 under the form of Equation 32 and changing the kinetic parameters of the slow reactions 5, 6 and 7 implied in nickel deposition as indicated in the relevant caption. Two well-separated capacitive loops clearly appear, whose proper frequencies, 10 and 0.06 Hz, correspond to the relaxations of $\mathscr{C}_0$ and θ_1 respectively. Then the clear-cut separation becomes even more pronounced than on diagram C in Fig. 5. On the other hand, with these parameters an equivalent quality of agreement is obtained between this modified model and our experimental results for the polarization curves, the nickel content of deposits and the impedance components. Consequently it is not yet possible to decide unambiguously between the two possible situations for the renewal of sites, i.e. either a nucleation governed by

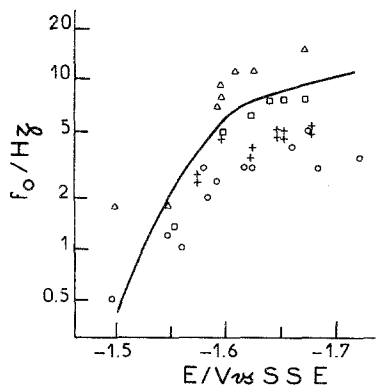

Fig. 13. Potential dependence of the frequency, f_0, at the apex of the medium-frequency capacitive loop. Solid line represents calculated curve with the same parameters as for Fig. 7. Experimental points with the same electrolytes as for Fig. 2: (○) electrolyte 1, $\Omega = 500\,\text{rev min}^{-1}$; (+) electrolyte 1, $\Omega = 1000\,\text{rev min}^{-1}$; (□) electrolyte 2, $\Omega = 1000\,\text{rev min}^{-1}$; (△) electrolyte 3, $\Omega = 1000\,\text{rev min}^{-1}$.

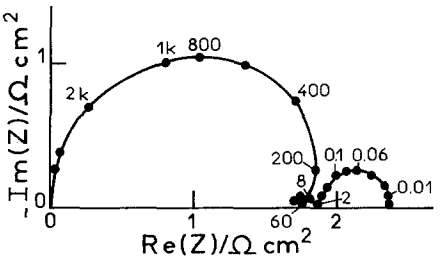

Fig. 14. Complex plane impedance plot calculated for interacting 's' sites according to Equation 32, with $g = 15$ and $\theta_0 = 0.09$. The parameters are those of Figs 7 and 10 except for $K_5 = 3.5 \times 10^{-9}\,\mathrm{cm^{-2}\,s^{-1}}$, $b_5 = 5\,\mathrm{V^{-1}}$, $K_6 = 1.5 \times 10^{-9}\,\mathrm{cm^{-2}\,s^{-1}}$ and $K_7 = 0$. Electrode polarization: $E = -1.7\,\mathrm{V}$, $i = 58\,\mathrm{mA\,cm^{-2}}$.

Equation 31 from independent $Ni(I)_{ads}$ coupled to an inclusion by reaction 7, or a formation according to Equation 32 from $Ni(I)_{ads}$ which interact when θ_2 exceeds θ_0.

5. Conclusion

By means of impedance spectroscopy the mechanism of Cu–Ni alloy deposition has been investigated in complexing citrate–ammonia electrolytes in which the discharge of cupric species is considerably inhibited.

Using a rotating disc electrode, it has been confirmed that the discharge of Cu(II)Cit is diffusion-controlled during Cu–Ni alloy deposition, thus generating a capacitive feature at medium frequencies. Impedance spectra, and particularly this capacitive feature, also agree with a two-step discharge of complexed cupric species where the first step has a much lower rate constant than the second one. An inductive feature and the potential dependence of the transfer resistance are shown to be consistent with a two-step discharge of nickel cations, Ni(II), involving a monovalent adsorbate $Ni(I)_{ads}$ originating from a first step whose reversibility is important.

A number of experimental relaxation processes and their potential dependences are semi-quantitatively in agreement with a reaction model where nickel and copper discharges are considered to occur in parallel at the electrode. In addition to likely changes in ion activities due to the presence of both Cu(II)Cit and Ni(II) in the electrolyte, an important effect of alloy deposition is the permanent renewal of active sites, s, which catalyse the reactions for nickel deposition. The slow renewal of these sites nucleated from $Ni(I)_{ads}$ on the alloy surface generates a low-frequency feature which is inductive at low electrode polarizations and becomes capacitive at high polarizations. The existence of a surface concentration maximum of sites as a function of potential suggests that these sites might have the particular reactivity of clusters made of one nickel atom bound to several copper atoms.

This reaction model reproduces the partial and total polarization curves, and also the dependence of the nickel content of the alloys upon the electrode polarization, fairly well.

References

[1] K. Vu Quang, B. Le Viet, E. Chassaing, J. P. Celis and J. R. Roos, *Metal Finishing* **10** (1985) 25.
[2] K. Vu Quang, E. Chassaing and M. Cherkaoui, Proceedings of INCEF-86, Bangalore, India, The Electrochemical Society of India, 20–26 February (1986).
[3] A. A. El Samahy, F. M. El Cheikh and I. S. Khedr, *J. Indian Chem. Soc.* **52** (1975) 752.
[4] M. F. M. Ghandour and A. Baraka, *Metalloberflaeche* **34** 10 (1980) 12.
[5] J. R. Roos, J. P. Celis, C. Buelens and D. Goris, in 'Application of Polarization Measurements in the Control of Metal Deposition', Process Metallurgy Vol. 3 (edited by I. Warren), Elsevier, Amsterdam (1984) p. 177.
[6] E. Chassaing, K. Vu Quang and R. Wiart, *J. Appl. Electrochem.* **16** (1986) 591.
[7] G. Charlot, 'Analyse Quantitative Minérale', Masson, Paris (1966) p. 721.
[8] I. Epelboin, M. Joussellin and R. Wiart, *J. Electroanal. Chem.* **119** (1981) 61.
[9] K. S. Cole, 'Membranes, Ions and Impulses', University of California Press, Berkeley (1968) p. 183.
[10] B. V. Tilak and B. E. Conway, *Electrochim Acta* **21** (1976) 719.
[11] T. Hepel, *J. Electroanal. Chem.* **175** (1984) 15.